

Revisiting multi-GNSS Navigation for UAVs – An Equivariant Filtering Approach

Martin Scheiber^{1*} , Alessandro Fornasier^{1*} , Christian Brommer¹ , and Stephan Weiss¹ 

Abstract—In this work, we explore the recent advances in equivariant filtering for inertial navigation systems to improve state estimation for uncrewed aerial vehicles (UAVs). Traditional state-of-the-art estimation methods, e.g., the multiplicative Kalman filter (MEKF), have some limitations concerning their consistency, errors in the initial state estimate, and convergence performance. Symmetry-based methods, such as the equivariant filter (EqF), offer significant advantages for these points by exploiting the mathematical properties of the system - its symmetry. These filters yield faster convergence rates and robustness to wrong initial state estimates through their error definition. To demonstrate the usability of EqFs, we focus on the sensor-fusion problem with the most common sensors in outdoor robotics: global navigation satellite system (GNSS) sensors and an inertial measurement unit (IMU). We provide an implementation of such an EqF leveraging the semi-direct product of the symmetry group to derive the filter equations. To validate the practical usability of EqFs in real-world scenarios, we evaluate our method using data from all outdoor runs of the *INSANE Dataset*. Our results demonstrate the performance improvements of the EqF in real-world environments, highlighting its potential for enhancing state estimation for UAVs.

I. INTRODUCTION

Since the dawn of autonomous micro-uncrewed aerial vehicles (UAVs), filter-based state estimation has played a major role for observer design. The extended Kalman filter (EKF) and its variants provide the possibilities to safely navigate UAVs in most environments by fusing measurements of (multiple) sensors. However, these approaches can suffer from large state errors in certain scenarios due to their simplified uncertainty handling and state-dependent linearization of the non-linear system dynamics [1].

In recent years, the aerial vehicles community has seen the advent of filter-based solutions that exploit the symmetries of the underlying dynamical system to design more robust filter. In this regard, the equivariant filter (EqF) has emerged as general filter design technique for systems on homogeneous space with symmetries [2]–[6]. EqFs possess several advantages compared to other filter methods. By exploiting the

This work has received funding from the European Union’s Horizon 2020 research and innovation programme under grant agreement 871260 (BugWright2), and was sponsored by the Army Research Office under Cooperative Agreement Number W911NF-21-2-0245. The views and conclusions contained in this document are those of the authors and should not be interpreted as representing the official policies, either expressed or implied, of the Army Research Office or the U.S. Government. The U.S. Government is authorized to reproduce and distribute reprints for Government purposes notwithstanding any copyright notation herein.

¹All authors are with Institute of Smart Systems Technologies, Control of Networked Systems Group, University of Klagenfurt, Universitätsstraße 65-67, 9020 Klagenfurt, Austria. Email: {first.lastname}@ieee.org.

* A. Fornasier and M. Scheiber contributed equally.

Pre-print version, accepted to ICAR23 in Oct/2023, DOI follows ASAP ©IEEE.

system’s underlying symmetry and lifting the system onto the symmetry group, the equivariant filter framework provides a natural choice of global state error with improved linearized error dynamics. Because of this, EqFs has a wider basin of attraction yielding high robustness to wrong initial conditions, and filter convergence regardless of their initial estimate [7]. Moreover, EqFs are shown to be naturally consistent even in the presence of unobservable states, which is in stark contrast to EKF-like approaches [8]–[10] and even in contrast to the “imperfect invariant EKF (IEKF)” [11] where some states, in particular the sensor biases, are “tacked-on” to the symmetry due to the approach’s limitations [12].

Nowadays, UAV manufacturers rely on multi-sensor fusion for their state estimation. When available, commercial products tend to fuse multiple global navigation satellite system (GNSS) measurements for more precise state estimation and redundancy. Yet, to the best of our knowledge, EqF formulations are not yet widely explored despite their mentioned advantages.

With this work, we present an implementation of a multi-position EqF formulation and compare its performance to state-of-the-art. We will show the advantages of EqF-based approaches for their consistency and state convergence in real-world scenarios. It will become particularly apparent that the EqF yields good results for poorly observable states with low signal-to-noise measurements caused by the scenario and trajectory [13], [14].

II. RELATED WORK

Many current plug-and-play frameworks rely on the EKF-based estimation and its derivatives [15]–[19].

Sasiadek et al. [20] introduced the formulation of combining GNSS measurements within an inertial navigation system (INS) for UAVs in a Kalman filter (KF). While this approach presents the KF based on the GNSS signal, they do not consider the rigid body sensor (self-)calibration or multi-GNSS sensor setups. Modern EKF-based approaches, which went from fusing single sensor types with calibrations [21] to extended states multi-sensor fusion [22], [23], take these into account.

Despite its success, the EKF is known to yield poor performance and inconsistencies for high linearization error in all situations where the motion leads to unobservability of the state vector [1]. To overcome issues related to high attitude linearization error and wrong initial attitude, in the eighties, *Lefferts et al.* [24], [25] explored the quaternion

group as parametrization of the attitude, introducing the so-called multiplicative EKF (MEKF), an algorithm that exploits the geometry of the rotational kinematics and is proven to outperform its EKF counterpart.

Following this trend, different authors exploited the underlying symmetry of the system to design robust observers and filters. *Barrau and Bonnabel* [8], [11] introduced the IEKF, an algorithm that exploits the natural symmetry of group affine systems, and directly models the state space onto a Lie group. In the context of inertial navigation systems, the IEKFs on $SE_2(3)$ proved superior to any EKF-like filter in terms of performance and consistency, in particular, for GNSS-based navigation the IEKF [26]–[28] outperform state-of-the-art solutions and to solve the inconsistencies typical to EKFs. That is, the spurious information gain, e.g., when the platform is not moving [1].

In recent years the EqF was proposed as a *general filter design* for systems with symmetry [3], [4] with specialization to the IEKF for group affine systems [4, Appendix B]. That is, the EqF approach is more general and applicable to a wider range of systems than the IEKF approach, as the latter one cannot properly include bias terms into the symmetry. Thus, leveraging the extended capabilities of EqFs, *Fornasier et al.* [7], [12], [29] introduced a symmetry for inertial navigation systems, that properly models inertial measurement unit (IMU) biases, and an associated EqF design. This work shows performance improvements compared to state-of-the-art IEKFs in terms of transient behavior - meaning the convergence phase of the filter - and robustness to wrong initial conditions.

This paper builds upon the latest results in equivariant filter design for inertial navigation system and introduces an equivariant filter formulation for *multiple* GNSS sensors, including their *individual extrinsic calibration states*. Therefore, leveraging the robustness and consistency properties of equivariant filters, we design and present an EqF that can be initialized arbitrarily, requiring no knowledge about the sensor's calibration states. We will show the performance advantages of using an EqF in real-world environments by evaluating our filter of the recently published *INSANE Dataset* [30], which includes a large quantity of outdoor flights with multiple GNSS sensors and high-rate position and orientation ground-truth. Due to the lack of open-source implementations of the IEKF, we will provide a comparison to a robust, openly available implementation of a MEKF [23].

In the following sections, we first present the mathematical operators for Lie groups and its Lie algebra (Sec. III), then introduce the biased-INS and its symmetry (Sec. IV-V), formulate the EqF (Sec. VI), and evaluate it on the *INSANE Dataset* [30] (Sec. VII-B). For the interested reader, in the appendix (App. A), we also recall the difference between the proposed EqF and the IEKF.

III. MATHEMATICAL PRELIMINARIES

The following section introduces the notation and mathematical preliminaries used in this paper. In general, bold

lowercase letters are used to indicate vectors, and bold capital letters are used to indicate matrices. Non-bold letters indicate elements of a symmetry group.

${}^A\mathbf{p}_B$ denotes the translation between reference frame $\{A\}$ and reference frame $\{B\}$, ${}^A\mathbf{v}_B$ denotes the corresponding velocity. All vectors referenced in $\{A\}$ are generally denoted by ${}^A\mathbf{p}$. Further, the rotation matrix rotating a vector from $\{B\}$ to $\{A\}$ is denoted by ${}^A\mathbf{R}_B$, i.e. ${}^A\mathbf{p} = {}^A\mathbf{R}_B {}^B\mathbf{p}$.

In what follows we quickly introduce some mathematical concepts about Lie groups that we used in this work. For an introduction of Lie groups theory for state estimation and robotics the reader is referred to *Solà et al.* [31].

Let \mathbf{G} be a Lie group, and \mathfrak{g} its Lie Algebra which is isomorphic with a vector space \mathbb{R}^n . We further define the following operators:

a) *Wedge and Vee Map*: The wedge map is defined as a map from the vector space to the Lie algebra,

$$(\cdot)^\wedge : \mathbb{R}^n \rightarrow \mathfrak{g},$$

and its inverse, the vee map, is defined as

$$(\cdot)^\vee : \mathfrak{g} \rightarrow \mathbb{R}^n.$$

b) *Adjoint Representations*: Given $X \in \mathbf{G}$ and $\mathbf{u}, \mathbf{v} \in \mathfrak{g}$, we define the Adjoint map $\text{Ad} : \mathbf{G} \times \mathfrak{g} \rightarrow \mathfrak{g}$ as

$$\text{Ad}_X[\mathbf{u}^\wedge] = dL_X dR_{X^{-1}}[\mathbf{u}^\wedge].$$

Further, in context of Lie matrix groups we define the Adjoint matrix map as

$$\text{Ad}_X^\vee(\mathbf{u}) = (\text{Ad}_X[\mathbf{u}^\wedge])^\vee.$$

Similarly the adjoint map $\text{ad} : \mathfrak{g} \rightarrow \mathfrak{g}$ and the adjoint matrix map for Lie matrix groups can be defined

$$\begin{aligned} \text{ad}_{\mathbf{u}^\wedge}[\mathbf{v}^\wedge] &= \mathbf{u}^\wedge \mathbf{v}^\wedge - \mathbf{v}^\wedge \mathbf{u}^\wedge, \\ \text{ad}_{\mathbf{u}^\wedge}^\vee(\mathbf{v}) &= (\mathbf{u}^\wedge \mathbf{v}^\wedge - \mathbf{v}^\wedge \mathbf{u}^\wedge)^\vee. \end{aligned}$$

IV. BIASED INERTIAL NAVIGATION SYSTEM

For this work, we consider an UAV equipped with an IMU measuring the robot's angular velocity and linear acceleration. Further, we consider the UAV to have N uncalibrated GNSS sensors onboard, each providing global position measurements. We define $\{G\}$ as the global inertial frame of reference, and $\{I\}$ as the body-fixed IMU frame of reference. The well-known, deterministic, dynamics of the biased inertial navigation system can then be written as

$${}^G\dot{\mathbf{R}}_I = {}^G\mathbf{R}_I ({}^I\boldsymbol{\omega} - {}^I\mathbf{b}_\omega)^\wedge, \quad (1a)$$

$${}^G\dot{\mathbf{v}}_I = {}^G\mathbf{R}_I ({}^I\mathbf{a} - {}^I\mathbf{b}_a) + {}^G\mathbf{g}, \quad (1b)$$

$${}^G\dot{\mathbf{p}}_I = {}^G\dot{\mathbf{v}}_I, \quad (1c)$$

$${}^I\dot{\mathbf{b}}_\omega = \mathbf{0}, \quad (1d)$$

$${}^I\dot{\mathbf{b}}_a = \mathbf{0}. \quad (1e)$$

${}^G\mathbf{R}_I$ refers to the rotation of the IMU, and ${}^G\mathbf{p}_I$ and ${}^G\mathbf{v}_I$ correspond to the IMU position and velocity in the global frame $\{G\}$. ${}^I\boldsymbol{\omega}$ and ${}^I\mathbf{a}$ are the body-fixed, biased inputs from the IMU and refer to the angular velocity and linear

acceleration, respectively, with its biases defined as ${}^I\mathbf{b}_\omega$ and ${}^I\mathbf{b}_a$. ${}^G\mathbf{g} = [0, 0, 9.81]^T \text{ m/s}^2$ refers to the gravity vector expressed in the global frame.

Let the core state space be defined as $\mathcal{C} = \mathcal{SO}(3) \times \mathbb{R}^{12}$ and the core state be defined as

$$\zeta = ({}^G\mathbf{R}_I, {}^G\mathbf{v}_I, {}^G\mathbf{p}_I, {}^I\mathbf{b}_\omega, {}^I\mathbf{b}_a) \in \mathcal{C}.$$

Let a zero-dynamic individual calibration state be defined as

$$\varsigma_i = ({}^I\mathbf{p}_{P_i}) \in \mathbb{R}^3,$$

with

$${}^I\dot{\mathbf{p}}_{P_i} = \mathbf{0}. \quad (2)$$

Then the full state in the state space $\mathcal{M} = \mathcal{C} \times (\mathbb{R}^3)^N$ can be defined as

$$\xi = (\zeta, \varsigma_1, \dots, \varsigma_N) \in \mathcal{M}.$$

We define the system's state space as $\xi = (\mathbf{T}, \mathbf{b}, \mathbf{t}_1, \dots, \mathbf{t}_N) \in \mathcal{M}$, where $\mathbf{T} = ({}^G\mathbf{R}_I, {}^G\mathbf{v}_I, {}^G\mathbf{p}_I) \in \mathcal{SE}_2(3)$ denotes the UAV's extended pose, $\mathbf{b} = ({}^I\mathbf{b}_\omega, {}^I\mathbf{b}_a) \in \mathbb{R}^6$ the IMU's biases, and $\mathbf{t}_i = {}^I\mathbf{p}_{P_i} \in \mathbb{R}^3$ the i -th sensor's calibration state. Further, $\mathbf{u} = ({}^I\boldsymbol{\omega}, {}^I\mathbf{a}) \in \mathbb{L} \subseteq \mathbb{R}^6$ describes the system's input. To simplify the notation in the subsequent sections the frame indices $\{G\}$, $\{I\}$, and $\{P_i\}$ are omitted.

Then the system described in (1a-1e) and (2) can be rewritten as

$$\dot{\mathbf{T}} = \mathbf{T}(\mathbf{W} - \mathbf{B} + \mathbf{D}) + (\mathbf{G} - \mathbf{D})\mathbf{T} \quad (3a)$$

$$\dot{\mathbf{b}} = \mathbf{0} \quad (3b)$$

$$\dot{\mathbf{t}}_i = \mathbf{0}, \quad (3c)$$

where

$$\begin{aligned} \mathbf{W} &= \begin{bmatrix} \boldsymbol{\omega}^\wedge & \mathbf{a} & \mathbf{0}_{3 \times 1} \\ \mathbf{0}_{2 \times 5} & & \end{bmatrix} \in \mathfrak{se}_2(3) \subset \mathbb{R}^{5 \times 5}, \\ \mathbf{B} &= \begin{bmatrix} \mathbf{b}_\omega^\wedge & \mathbf{b}_a & \mathbf{0}_{3 \times 1} \\ \mathbf{0}_{2 \times 5} & & \end{bmatrix} \in \mathfrak{se}_2(3) \subset \mathbb{R}^{5 \times 5}, \\ \mathbf{G} &= \begin{bmatrix} \mathbf{0}_{3 \times 3} & \mathbf{g} & \mathbf{0}_{3 \times 1} \\ \mathbf{0}_{2 \times 5} & & \end{bmatrix} \in \mathfrak{se}_2(3) \subset \mathbb{R}^{5 \times 5}, \text{ and} \\ \mathbf{D} &= \begin{bmatrix} \mathbf{0}_{3 \times 4} & \mathbf{0} \\ \mathbf{0}_{1 \times 4} & 1 \\ \mathbf{0}_{1 \times 4} & \mathbf{0} \end{bmatrix} \in \mathbb{R}^{5 \times 5}. \end{aligned}$$

To simplify notation, in the following sections, the elements related to the position sensors (calibrations) are denoted only once with index i . Please note that for N sensors, $1 \leq i \leq N$, these elements would be repeated N times.

V. SEMI-DIRECT PRODUCT SYMMETRY

In this section, we present the symmetry of the previously defined system. The symmetry is based on the semi-direct product group $\text{SE}_2(3) \ltimes \mathfrak{se}(3)$ [32], [33] and builds upon the author's previous work [7], [29].

Given the revised system dynamics in (3a-3c), we define the symmetry group to be $\mathbf{G} := (\text{SE}_2(3) \ltimes \mathfrak{se}(3)) \ltimes (\mathbb{R}^3)^N$.

Let $X = (C, \gamma, d_i) \in \mathbf{G}$ be an element of the symmetry group, with $C = (B, b) \in \text{SE}_2(3)$ and $B = (A, a) \in \text{SE}(3)$. Then the inverse element is given by $X^{-1} = (C^{-1}, -\text{Ad}_{B^{-1}}[\gamma], -A^T d_i)$ with $C^{-1} = (A^T, -A^T a, -A^T b)$, and the identity element of \mathbf{G} is $\text{id} = (\mathbf{I}_3, \mathbf{0}, \mathbf{0}, \mathbf{0}) \in \mathbf{G}$.

A. Equivariance

This section presents the group action and equivariant configuration output required for the later EqF design.

Definition 5.1. The transitive right group action of \mathbf{G} on \mathcal{M} , $\phi : \mathbf{G} \times \mathcal{M} \rightarrow \mathcal{M}$ for our filter is defined as

$$\phi(X, \xi) := (\mathbf{T}C, \mathbf{A}\mathbf{d}_{B^{-1}}^\vee(\mathbf{b} - \gamma^\vee), A^T(\mathbf{t}_i - d_i)) \in \mathcal{M}. \quad (4)$$

Definition 5.2. Given the defined measurement equation $y_i = h_i(\xi) \in \mathcal{N}$ of a known vector quantity $\boldsymbol{\delta}_i$ with [29]

$$h_i(\xi) = \mathbf{R}^T(\boldsymbol{\delta}_i - (\mathbf{p} + \mathbf{R}\mathbf{t}_i)), \quad (5)$$

for $1 \leq i \leq N$. Then the equivariant configuration output of our filter, $\rho : \mathbf{G} \times \mathcal{N} \rightarrow \mathcal{N}$ can be defined as

$$\rho_i(X, y_i) := A^T(y_i - b + d_i). \quad (6)$$

In the EqF design below, the vector $\boldsymbol{\delta}_i$ is set to zero.

B. Equivariant Lift

In the context of equivariant filtering the lift [2] provides the structure that connects the input of the system posed on the homogeneous space to the input of the system lifted onto the symmetry group. For the given system in (3a-3c) the lift is defined as follows.

Definition 5.3. We define the map $\Lambda(\xi, \mathbf{u}) = (\Lambda_I(\xi, \mathbf{u}), \Lambda_{II}(\xi, \mathbf{u}), \Lambda_i(\xi, \mathbf{u}))$ as a lift for the system defined in (3a-3c) with

$$\Lambda_I(\xi, \mathbf{u}) := (\mathbf{W} - \mathbf{B} + \mathbf{D}) + \mathbf{T}^{-1}(\mathbf{G} - \mathbf{D})\mathbf{T} \quad (7a)$$

$$\Lambda_{II}(\xi, \mathbf{u}) := \text{ad}_{\mathbf{b}^\wedge}[\Pi(\Lambda_I(\xi, \mathbf{u}))] \quad (7b)$$

$$\Lambda_i(\xi, \mathbf{u}) := -(\boldsymbol{\omega} - \mathbf{b}_\omega)^\wedge \mathbf{t}_i \quad i = 1, \dots, N \quad (7c)$$

where $\Lambda_1 : \mathcal{M} \times \mathbb{L} \rightarrow \mathfrak{se}_2(3)$, $\Lambda_2 : \mathcal{M} \times \mathbb{L} \rightarrow \mathfrak{se}(3)$, and $\Lambda_i : \mathcal{M} \times \mathbb{L} \rightarrow \mathbb{R}^3$. $\Pi : \mathfrak{se}_2(3) \rightarrow \mathfrak{se}(3)$ is a map defined such that, $\forall \mathbf{x}, \mathbf{y}, \mathbf{z} \in \mathbb{R}^3 | (\mathbf{x}, \mathbf{y}, \mathbf{z}) \in \mathbb{R}^9$, $\Pi((\mathbf{x}, \mathbf{y}, \mathbf{z})^\wedge) = (\mathbf{x}, \mathbf{y})^\wedge \in \mathfrak{se}(3)$.

VI. EQUIVARIANT FILTER DESIGN

We extend the filter design of our previous work [7], [12], [29] with the presented symmetries given measurements from an IMU propagation sensor and N GNSS position update sensors. Similar to our previous work, we initialize the filter to the origin of the state space $\hat{\xi} = \text{id}$.

We further define local coordinates ε for the equivariant error $e := \phi(\hat{X}^{-1}, \xi)$, to be normal coordinates, thus $\varepsilon = \vartheta(e) := \log(\phi_\xi^{-1}(e))^\vee \in \mathbb{R}^n$, where $\log : \mathbf{G} \rightarrow \mathfrak{g}$ is the logarithm of the symmetry group. Note that given the EqF estimate in the symmetry group at time t , that is $\hat{X}(t)$, the system's estimate at time t is written $\hat{\xi}(t) = \phi(\hat{X}(t), \hat{\xi})$ [4].

We can derive the linearized error state, and output matrices

$$\dot{\varepsilon} \simeq \mathbf{A}_t^0 \varepsilon, \quad (8)$$

$$\delta(h(e)) = \delta\left(\rho\left(\hat{X}^{-1}, h(\xi)\right)\right) \approx \mathbf{C}_t^* \varepsilon, \quad (9)$$

where \mathbf{A}_t^0 and \mathbf{C}_t^* are defined according to [29].

When formulating filters for real-world data, one cannot assume all sensors' measurements to be available simultaneously. The following presents a general filter formulation applying updates for the i -th position sensor. This formulation allows an arbitrary number of sensor updates at different rates, as in real-world environments.

Let $\varepsilon = \vartheta(e) = (\varepsilon_{\mathbf{R}}, \varepsilon_{\mathbf{v}}, \varepsilon_{\mathbf{p}}, \varepsilon_{\mathbf{b}}, \varepsilon_{\mathbf{t}_i}) \in \mathbb{R}^{18}$ and using the previous equations, we can then derive the linearized filter matrices for the i -th sensor update as

$$\mathbf{A}_t^0 = \begin{bmatrix} \Upsilon_1 & \Upsilon_2 & \mathbf{0}_{9 \times 3N} \\ \mathbf{0}_{6 \times 9} & \Upsilon_3 & \mathbf{0}_{6 \times 3N} \\ \mathbf{0}_{3N \times 9} & \mathbf{0}_{3N \times 6} & \Upsilon_4 \end{bmatrix} \in \mathbb{R}^{(15+3N) \times (15+3N)} \quad (10)$$

$$\mathbf{C}_{t,i}^* = [\Upsilon_5 \quad \mathbf{0}_{3 \times 3} \quad -\mathbf{I}_3 \quad \mathbf{0}_{3 \times 6} \quad \Upsilon_6] \in \mathbb{R}^{3 \times (15+3N)} \quad (11)$$

where,

$$\Upsilon_1 = \begin{bmatrix} \mathbf{0}_{3 \times 3} & \mathbf{0}_{3 \times 3} & \mathbf{0}_{3 \times 3} \\ \mathbf{g}^\wedge & \mathbf{0}_{3 \times 3} & \mathbf{0}_{3 \times 3} \\ \mathbf{0}_{3 \times 3} & \mathbf{I}_3 & \mathbf{0}_{3 \times 3} \end{bmatrix} \in \mathbb{R}^{9 \times 9},$$

$$\Upsilon_2 = \begin{bmatrix} \mathbf{I}_6 \\ \hat{\mathbf{b}}^\wedge & \mathbf{0}_{3 \times 3} \end{bmatrix} \in \mathbb{R}^{9 \times 6},$$

$$\Upsilon_3 = \mathbf{ad}_{\mathbf{r}_7}^\vee \in \mathbb{R}^{6 \times 6},$$

$$\Upsilon_4 = \text{diag}(\Gamma_1, \dots, \Gamma_N) \in \mathbb{R}^{3N \times 3N},$$

$$\Upsilon_5 = \frac{1}{2}(y_i + \hat{\mathbf{b}} - \hat{\mathbf{d}}_i)^\wedge \in \mathbb{R}^{3 \times 3},$$

$$\Upsilon_6 = [\delta_{1,i} \mathbf{I}_3, \dots, \delta_{N,i} \mathbf{I}_3] \in \mathbb{R}^{3 \times 3N},$$

$$\Upsilon_7 = \mathbf{Ad}_B^\vee(\boldsymbol{\omega}) + \hat{\gamma}^\vee + \hat{\mathbf{G}} \in \mathfrak{se}_2(3) \subset \mathbb{R}^{4 \times 4}, \text{ and}$$

$$\Gamma_1 = \dots = \Gamma_n = (\hat{A} \boldsymbol{\omega} + \hat{\gamma}_\omega^\vee)^\wedge \in \mathbb{R}^{3 \times 3}.$$

$\delta_{j,i}$ refers to the Kronecker delta, which is 1 if $i = j$ and 0 otherwise. Thus, Υ_6 is a 3-by- $3N$ zero matrix, except the i -th 3-by-3 block being the identity matrix, corresponding to the i -th sensor update. $\hat{\mathbf{G}} \in \mathfrak{se}_2(3) \subset \mathbb{R}^{4 \times 4}$ refers to the upper-left 4-by-4 matrix of $\hat{\mathbf{G}}$.

Finally, our discrete-time EqF's propagation and update equations are quite similar to the one of an EKF [12].

$$\mathbf{S} = \mathbf{C}_{t,i}^* \Sigma_{k+1}^- \mathbf{C}_{t,i}^{*\top} + \mathbf{N}, \quad (12a)$$

$$\mathbf{K} = \Sigma_{k+1}^- \mathbf{C}_{t,i}^{*\top} \mathbf{S}^{-1}, \quad (12b)$$

$$\delta = \rho_i(\hat{X}^{-1}, 0) - y_i \quad (12c)$$

$$\Delta = D_E|_{\text{id}} \phi\left(\begin{smallmatrix} \hat{\xi} \\ E \end{smallmatrix}\right) d\vartheta^{-1} \cdot \mathbf{K} \delta \quad (12d)$$

$$\hat{X}_{k+1}^+ = \exp(\Delta) \hat{X}_{k+1}^-, \quad (12e)$$

$$\Sigma_{k+1}^+ = (\mathbf{I} - \mathbf{K} \mathbf{C}_{t,i}^*) \Sigma_{k+1}^-, \quad (12f)$$

where $\mathbf{N} \in \mathbb{S}_+(3) \subset \mathbb{R}^{3 \times 3}$ is an output gain matrix, and $\Sigma \in \mathbb{S}_+(15+3N) \subset \mathbb{R}^{15+3N \times 15+3N}$ the Riccati or covariance

matrix (of the error in local coordinates). $\hat{X} \in \mathbf{G}$ is the EqF state with the initial state $\hat{X}(0) = \text{id}$. The main difference to an EKF formulation is the definition of the innovation residual Δ , where $D_E|_{\text{id}} \phi\left(\begin{smallmatrix} \hat{\xi} \\ E \end{smallmatrix}\right) d\vartheta^{-1}$ maps the scaled residual $\mathbf{K} \delta$ into the Lie algebra of the symmetry group.

VII. EXPERIMENTAL EVALUATION

To evaluate our filter design and show the usability of real data, we use the *INSANE Dataset* [30]. This dataset provides recordings with over 14 sensors, including two GNSS sensors offset by approx. 1 m from the IMU. To show the usability of the proposed filter, we use the 19 “Mars” (outdoor) and the “Outdoor” recordings of the *INSANE Dataset*. We select this dataset as it includes a wide range of UAV flights, from long-distance to short pickup-and-place, high-speed to low-speed flights. It also contains an outdoor orientation ground-truth, which is derived geometrically from raw sensor measurements using the vehicle's geometry and sensors' calibration.

Note that, due to external influences in this dataset not all flights have a highly accurate RTK-GNSS fix available. Since these measurements are also used to generate the ground-truth orientation, slight position measurement errors can yield larger orientation errors, rendering the “ground-truth” less accurate. The affected datasets are marked with a star (*) in Table I.

A. Comparison to MEKF approaches

Due to the lack of open-source implementation of a IEKF - with neither single nor multiple-GNSS sensors - we choose to compare our presented filter to an implementation of a state-of-the-art modular MEKF [23] to have at least well-known comparison data. This MEKF implementation directly provides (multiple) GNSS sensor modules with very little modification. For a detailed performance analysis of the consistency and core error state performance we refer the reader to our previous work [29]. We further want to highlight that the MEKF formulation is able to handle asynchronous and out-of-order measurements, while the EqF implementation is designed in a simpler way to show the proof of concept.

We initialize both filters with the same initial state, i.e., $\hat{\xi} = \text{id} = (\mathbf{I}_3, \mathbf{0}, \mathbf{0}, \mathbf{0}, \mathbf{0}, \mathbf{0}) \in \mathcal{M}$. We want to highlight the purposely wrong chosen initial state for both GNSS sensor calibrations, whose ground-truth values are

$$\mathbf{t}_1 = [0.35, 0.41, 0]^\top \text{ m}$$

$$\mathbf{t}_2 = [-0.47, -0.41, 0]^\top \text{ m}.$$

Given that this initial estimate is most likely outside the beacon of convergence for the MEKF, we acknowledge that EKF-based approaches tend to require an initial state within the proximity off the ground-truth. However, with the wrong initial state estimate, we want to highlight the performance of symmetry-based approaches concerning the convergence and rate.

TABLE I
RMSE EVALUATION IN THE ASYMPTOTIC PHASE OF OUR EQF
FRAMEWORK COMPARED TO A MEKF-BASED IMPLEMENTATION ON THE
INSANE Dataset [30].

Dataset No.	t_0 [s]	EqF RMSE		MEKF RMSE	
		Pos. [m]	Att. [°]	Pos. [m]	Att. [°]
M01	20	0.1089	12.7486	0.5264	2.5468
M02	23	0.0890	3.8077	4.2120	128.5142
M03	29	0.1529	2.5925	5.6688	97.5796
M04*	34	0.3063	5.7552	2.4872	45.7479
M05	50	0.1449	1.9385	1.1497	8.0534
M06	25	0.0966	3.3420	0.1237	7.4513
M07	36	0.1766	2.7015	0.6316	11.5197
M08*	43	0.2205	9.0050	0.3291	11.9717
M09*	34	0.4682	10.8112	3.6165	38.2228
M10	42	0.2332	6.4940	1.2518	12.9468
M11	31	0.3415	5.7310	2.4224	36.0030
M12	27	0.3705	2.8902	1.7011	10.4460
M13	10	0.1957	3.1973	2.7391	76.1869
M14*	45	0.8265	28.5057	2.7604	60.5424
M15	14	0.2452	4.1148	2.3284	30.6290
M16*	42	0.1955	6.9932	0.2311	6.8966
M17*	35	0.1660	6.9044	3.1691	50.2471
M18*	54	0.1289	9.0023	0.5740	19.1046
M19*	23	0.1217	4.3011	1.3056	6.3813
O01*	50	0.2251	11.3116	0.8893	17.4661

Further, both filters are initialized with the same state covariance Σ_0 and use the same measurement noise.

B. Evaluation Results

We evaluate the 20 above-mentioned recordings of the *INSANE Dataset* on both filter frameworks. Due to the long static duration at the beginning of each recording and the known observability/consistency issues for EKF-based frameworks, an empirically derived starting time t_0 was chosen for each evaluation (c.f. Table I) in favor of the MEKF approach. As it is known in EKF-based approaches, noisy position measurements from off-center sensors can lead to incorrect yaw estimation when there is no motion present. Thus, for a fair comparison, we want to limit this effect only to the motion-full part of the dataset.

The RMSE of each individual evaluation is given in Table I. As expected, the EqF performs well in most datasets compared to MEKF approaches. We can further show that, without any knowledge of the sensor calibration, i.e., initializing these states at identity, the EqF performs well for all flights of the *INSANE Dataset*. For interested readers, we also provide the trajectory comparison of all runs in App. B.

Furthermore, for the selected dataset *Mars 5 (M05)*, we compare the pose errors for the EqF and MEKF implementation in Fig. 1 with the calibration state and bias estimates displayed in Fig. 2 and Fig. 3, respectively. We choose this dataset as it represents a low signal-to-noise ratio scenario with generally little excitation and thus decreased yaw observability throughout the entire run.

In this comparison, we can clearly see the advantages of the EqF framework. Both frameworks are able to converge to a good orientation estimate, though the MEKF has a



Fig. 1. Pose error for the EqF and MEKF frameworks on dataset M05.

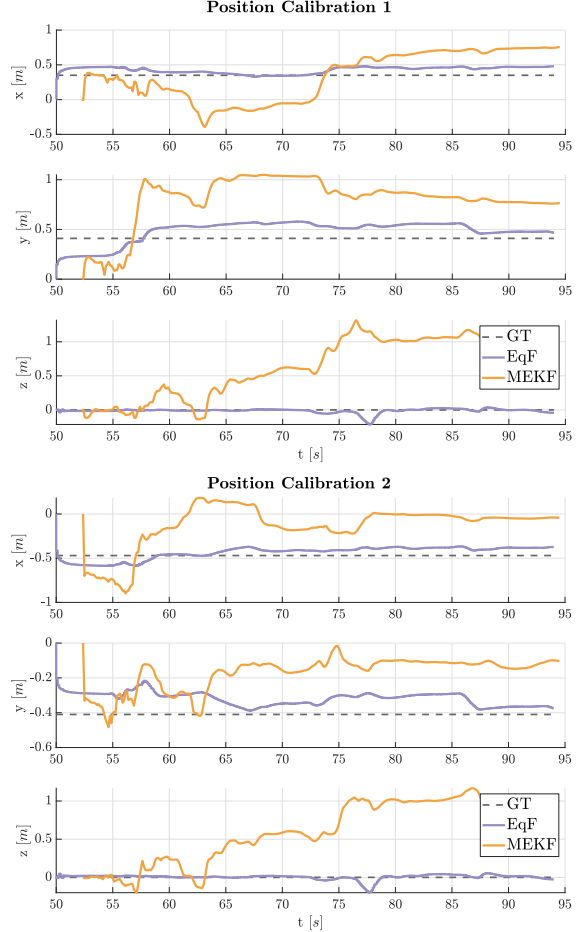


Fig. 2. Calibration states comparison between the EqF and MEKF frameworks and ground-truth ("GT") on flight M05. Both frameworks are intentionally initialized with a wrong calibration, $\hat{\mathbf{t}}_1(t_0) = \hat{\mathbf{t}}_2(t_0) = \mathbf{0}$. Yet, the EqF framework can converge to the correct states (faster) in contrast to the MEKF-based approach.

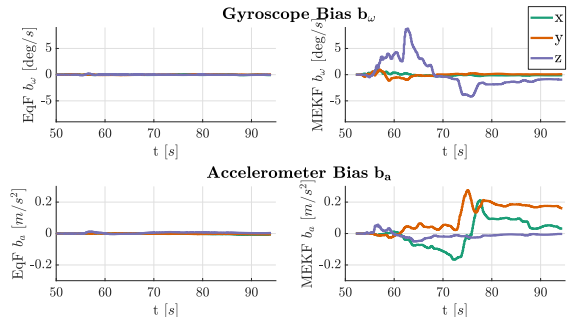


Fig. 3. Bias estimates of the EqF and MEKF frameworks on dataset M05.

noticeable longer convergence time. However, as can be expected, while improving on the orientation estimate the MEKF trades the position accuracy as its calibration states are not converging correctly. The EqF converges fast and correctly to the actual sensor calibrations. As a result, the EqF is able to provide accurate state estimates even if the rigid body sensor calibrations are initially completely unknown.

For the sake of completeness, we acknowledge and tested the MEKF with initial states only 5 % off ground-truth values and we were able to achieve similar estimation results as the EqF. Naturally, the low initial error reduces the linearization error in the MEKF approach improving its performance. The benefit of the EqF formulation is, indeed, in the much faster transient, larger beacon of attraction, and consistency rather than in the asymptotic behavior.

For consistency evaluation, we further present the filter energy (or NEES [10]) for M05 in Fig. 4. For this, we consider the states with available ground-truth, i.e., position, orientation, and both calibration states. For more details on this evaluation and comparisons to many other filter setups we refer the reader to [29]. In this evaluation, we clearly see the EqF’s filter energy converging to a magnitude of 1. However, the MEKF is several order of magnitudes higher, resulting in an over-confident system. We observe this behavior throughout all evaluations of the *INSANE Dataset*.

VIII. SUMMARY

With this contribution we provide an EqF framework for multi-GNSS setups for UAVs, which takes advantages of a Lie symmetry group for lifting the system dynamics. We further show that this type of filter formulation yields improved performance compared to the currently most commonly used MEKFs. This is a result of the better system formulation and its inherited properties for convergence, linearization errors, and consistency. When evaluated on multiple runs of the *INSANE Dataset*, the proposed filter is able to correctly estimate the vehicle’s pose and all GNSS extrinsic calibration states throughout all flights.

Overall, this work aims to serve as a basis for future multi-sensor EqF frameworks and provide the initial formulation on how a multi-GNSS setup within a biased-inertial navigation system can be formulated equivariantly.

APPENDIX A DIFFERENCES WITH IEKF

In this section we highlight the major differences between the proposed EqF and the IEKF. For an in-depth discussion on the topic, we refer the reader to our very recent research [29].

The IEKF is a filter design for systems with group affine dynamics on a Lie group [11]. The EqF, instead, can be seen as a general filter design for systems with symmetries, where the original system is lifted onto a Lie group, the symmetry group, and a filter is designed based on the equivariant error. The EqF specializes to the IEKF for systems with group affine dynamics on a Lie group, when the Lie group is chosen

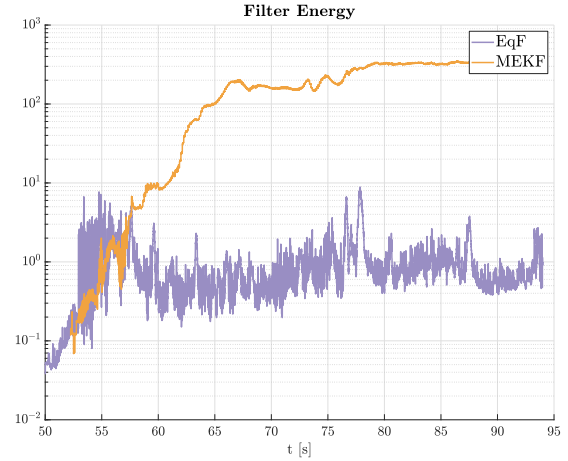


Fig. 4. Filter energy comparison between the EqF and MEKF frameworks on flight M05. In this run, the MEKF is over-confident given its position and calibration state errors. The EqF converges to magnitude of 1 as is expected of consistent filters.

as symmetry group, the origin is chosen to be the identity, and the local coordinates are chosen to be the logarithmic coordinates [4, Appendix B].

Previous work has introduced a variant of the IEKF, coined the “imperfect-IEKF” [1], to handle this type of problem. This paper addresses the problem of filter design for a biased inertial navigation system, as depicted in (1a-1e), which does not possess group affine dynamics. In the imperfect-IEKF, the IMU biases are treated as elements of a Euclidean space attached to the navigation group, resulting in a Lie group structure of $SE_2(3) \times \mathbb{R}^6$. In contrast, our proposed EqF exploits the semi-direct product symmetry $SE_2(3) \ltimes \mathfrak{se}(3)$ proposed in [7], [29], resulting in a filter with identical error dynamics for attitude, position, and velocity (Υ_1 in (10)), while introducing distinct error dynamics for IMU biases (Υ_2, Υ_3 in (10)), thereby improving the linearization error [29]. Additionally, by employing normal coordinates instead of logarithmic coordinates, the proposed EqF achieves a third-order linearization error reduction in the output linearization [4].

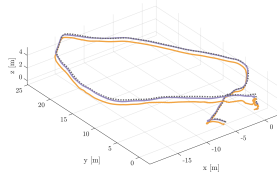
APPENDIX B INSANE EVALUATION

For completeness we provide the evaluation of the proposed EqF framework on all 19 “Mars” and the “Outdoor” flights of the *INSANE Dataset* [30]. The evaluation of each individual flight is shown in Fig. 5. With this evaluation, we can successfully demonstrate that an EqF framework performs successful state estimation in real-world environments.

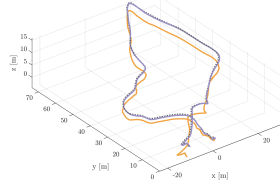
REFERENCES

- [1] A. Barrau, “Non-linear state error based extended Kalman filters with applications to navigation,” Dissertation, Automatic. Mines Paristech, 2015. <https://hal.science/tel-01247723>
- [2] R. Mahony, T. Hamel, and J. Trumpf, “Equivariant Systems Theory and Observer Design,” Aug. 2020, arXiv:2006.08276 [eess.SY]. <http://arxiv.org/abs/2006.08276>

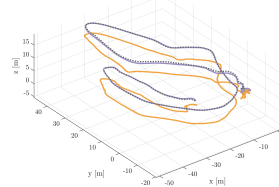
- [3] P. van Goor, T. Hamel, and R. Mahony, "Equivariant filter (EqF): A General Filter Design for Systems on Homogeneous Spaces," in *2020 59th IEEE Conference on Decision and Control (CDC)*. Jeju, Korea (South): IEEE, 2020, pp. 5401–5408, arXiv:2107.05193 [eess.SY]. <https://ieeexplore.ieee.org/document/9303813>
- [4] —, "Equivariant Filter (EqF)," *IEEE Transactions on Automatic Control*, vol. 68, no. 6, pp. 3501–3512, June 2023, arXiv:2010.14666 [eess.SY]. <https://ieeexplore.ieee.org/document/9840886/>
- [5] R. Mahony, P. van Goor, and T. Hamel, "Observer Design for Nonlinear Systems with Equivariance," *Annual Review of Control, Robotics, and Autonomous Systems*, vol. 5, no. 1, pp. 221–252, May 2022, arXiv:2108.09387 [eess.SY]. <https://www.annualreviews.org/doi/10.1146/annurev-control-061520-010324>
- [6] Y. Ng, P. van Goor, T. Hamel, and R. Mahony, "Equivariant Systems Theory and Observer Design for Second Order Kinematic Systems on Matrix Lie Groups," in *2020 59th IEEE Conference on Decision and Control (CDC)*. Jeju, Korea (South): IEEE, Dec. 2020, pp. 4194–4199, arXiv:2105.04797 [eess.SY]. <https://ieeexplore.ieee.org/document/9303761/>
- [7] A. Fornasier, Y. Ng, R. Mahony, and S. Weiss, "Equivariant Filter Design for Inertial Navigation Systems with Input Measurement Biases," in *2022 International Conference on Robotics and Automation (ICRA)*. Philadelphia, PA, USA: IEEE, 2022, pp. 4333–4339, arXiv:2202.02058 [cs.RO]. <https://ieeexplore.ieee.org/document/9811778>
- [8] A. Barrau and S. Bonnabel, "Invariant Kalman Filtering," *Annual Review of Control, Robotics, and Autonomous Systems*, vol. 1, no. 1, pp. 237–257, May 2018. <https://www.annualreviews.org/doi/10.1146/annurev-control-060117-105010>
- [9] K. Wu, T. Zhang, D. Su, S. Huang, and G. Dissanayake, "An invariant-EKF VINS algorithm for improving consistency," in *2017 IEEE/RSJ International Conference on Intelligent Robots and Systems (IROS)*. Vancouver, BC: IEEE, Sept. 2017, pp. 1578–1585. <http://ieeexplore.ieee.org/document/8205965/>
- [10] A. Fornasier, M. Scheiber, A. Hardt-Stremayr, R. Jung, and S. Weiss, "VINSEval: Evaluation Framework for Unified Testing of Consistency and Robustness of Visual-Inertial Navigation System Algorithms," in *2021 IEEE International Conference on Robotics and Automation (ICRA)*. Xi'an, China: IEEE, 2021, pp. 13 754–13 760. <https://ieeexplore.ieee.org/document/9561382/>
- [11] A. Barrau and S. Bonnabel, "The Invariant Extended Kalman Filter as a Stable Observer," *IEEE Transactions on Automatic Control*, vol. 62, no. 4, pp. 1797–1812, 2017. <http://ieeexplore.ieee.org/document/7523335/>
- [12] A. Fornasier, Y. Ng, C. Brommer, C. Böhm, R. Mahony, and S. Weiss, "Overcoming Bias: Equivariant Filter Design for Biased Attitude Estimation With Online Calibration," *IEEE Robotics and Automation Letters*, vol. 7, no. 4, pp. 12 118–12 125, 2022, arXiv:2209.12038 [cs.RO]. <https://ieeexplore.ieee.org/document/9905914/>
- [13] G. Teodori and H. Neuner, "Analysis of the Yaw Observability in GNSS-INS Integration for UAV Pose Estimation," in *Contributions to International Conferences on Engineering Surveying*. Cham: Springer International Publishing, 2021, p. 259269. https://link.springer.com/chapter/10.1007/978-3-030-51953-7_22
- [14] Y. Li, X. Niu, Y. Cheng, C. Shi, and N. El-Sheimy, "The Impact of Vehicle Maneuvers on the Attitude Estimation of GNSS / INS for Mobile Mapping," *Journal of Applied Geodesy*, vol. 9, no. 3, Jan. 2015. <https://www.degruyter.com/document/doi/10.1515/jag-2015-0002/html>
- [15] L. Meier, P. Tanskanen, F. Fraundorfer, and M. Pollefeys, "THE PIXHAWK OPEN-SOURCE COMPUTER VISION FRAMEWORK FOR MAVS," *The International Archives of the Photogrammetry, Remote Sensing and Spatial Information Sciences*, vol. XXXVIII-1/C22, pp. 13–18, Sept. 2012. <https://www.int-arch-photogramm-remote-sens-spatial-inf-sci.net/XXXVIII-1-C22/13/2011/>
- [16] S. Weiss and R. Siegwart, "Real-time metric state estimation for modular vision-inertial systems," in *2011 IEEE International Conference on Robotics and Automation*. Shanghai, China: IEEE, May 2011, pp. 4531–4537. <http://ieeexplore.ieee.org/document/5979982/>
- [17] "ArduPilot." <https://ardupilot.org/ardupilot/index.html>
- [18] T. Moore and D. Stouch, "A Generalized Extended Kalman Filter Implementation for the Robot Operating System," in *Intelligent Autonomous Systems 13*, ser. Advances in Intelligent Systems and Computing. Cham: Springer International Publishing, 2015, vol. 302, pp. 335–348. https://link.springer.com/10.1007/978-3-319-08338-4_25
- [19] "PX4." https://docs.px4.io/main/en/advanced_config/tuning_the_ecl_ekf.html
- [20] J. Sasiadek and P. Hartana, "Sensor fusion for navigation of an autonomous unmanned aerial vehicle," in *IEEE International Conference on Robotics and Automation, 2004. Proceedings. ICRA '04. 2004*. New Orleans, LA, USA: IEEE, 2004, pp. 4029–4034 Vol.4. <http://ieeexplore.ieee.org/document/1308901/>
- [21] S. Weiss, M. W. Achtelik, M. Chli, and R. Siegwart, "Versatile distributed pose estimation and sensor self-calibration for an autonomous MAV," in *2012 IEEE International Conference on Robotics and Automation*. St Paul, MN, USA: IEEE, 2012, pp. 31–38. <http://ieeexplore.ieee.org/document/6225002/>
- [22] S. Lynen, M. W. Achtelik, S. Weiss, M. Chli, and R. Siegwart, "A robust and modular multi-sensor fusion approach applied to MAV navigation," in *2013 IEEE/RSJ International Conference on Intelligent Robots and Systems*. Tokyo: IEEE, Nov. 2013, pp. 3923–3929. <http://ieeexplore.ieee.org/document/6696917/>
- [23] C. Brommer, R. Jung, J. Steinbrener, and S. Weiss, "MaRS: A Modular and Robust Sensor-Fusion Framework," *IEEE Robotics and Automation Letters*, vol. 6, no. 2, pp. 359–366, Apr. 2021. <https://ieeexplore.ieee.org/document/9286578/>
- [24] E. J. Lefferts, F. L. Markley, and M. D. Shuster, "Kalman filtering for spacecraft attitude estimation," *Journal of Guidance, Control, and Dynamics*, vol. 5, no. 5, pp. 417–729, 1982. <https://arc.aiaa.org/doi/10.2514/3.56190>
- [25] F. L. Markley, "Attitude Error Representations for Kalman Filtering," *Journal of Guidance, Control, and Dynamics*, vol. 26, no. 2, pp. 311–317, Mar. 2003. <https://arc.aiaa.org/doi/10.2514/2.5048>
- [26] N. Pavlasek, A. Walsh, and J. R. Forbes, "Invariant Extended Kalman Filtering Using Two Position Receivers for Extended Pose Estimation," in *2021 IEEE International Conference on Robotics and Automation (ICRA)*. Xi'an, China: IEEE, May 2021, pp. 5582–5588, arXiv:2104.14711 [cs.RO]. <https://ieeexplore.ieee.org/document/9561150/>
- [27] A. Barrau and S. Bonnabel, "Navigating with highly precise odometry and noisy GPS: a case study**This work is supported by the company Safran." *IFAC-PapersOnLine*, vol. 49, no. 18, pp. 618–623, 2016, hal: hal-01267244. <https://linkinghub.elsevier.com/retrieve/pii/S2405896316318146>
- [28] C. Liu, C. Jiang, and H. Wang, "InGVIO: A Consistent Invariant Filter for Fast and High-Accuracy GNSS-Visual-Inertial Odometry," *IEEE Robotics and Automation Letters*, vol. 8, no. 3, pp. 1850–1857, Mar. 2023, arXiv:2210.15145 [cs.RO]. <https://ieeexplore.ieee.org/document/10040716/>
- [29] A. Fornasier, Y. Ge, P. van Goor, R. Mahony, and S. Weiss, "Equivariant Symmetries for Inertial Navigation Systems," Sept. 2023, arXiv:2309.03765 [cs.RO]. <http://arxiv.org/abs/2309.03765>
- [30] C. Brommer, A. Fornasier, M. Scheiber, J. Delaune, R. Brockers, J. Steinbrener, and S. Weiss, "INSANE: Cross-Domain UAV Data Sets with Increased Number of Sensors for developing Advanced and Novel Estimators," 2022, arXiv:2210.09114 [cs.RO]. https://www.aau.at/wp-content/uploads/2022/10/brommer_insane_dataset.pdf
- [31] J. Solà, J. Deray, and D. Atchuthan, "A micro Lie theory for state estimation in robotics," Dec. 2021, arXiv:1812.01537 [cs.RO]. <http://arxiv.org/abs/1812.01537>
- [32] Y. Ng, P. van Goor, R. Mahony, and T. Hamel, "Attitude Observation for Second Order Attitude Kinematics," in *2019 IEEE 58th Conference on Decision and Control (CDC)*. Nice, France: IEEE, Dec. 2019, pp. 2536–2542, arXiv:2104.06596 [eess.SY]. <https://ieeexplore.ieee.org/document/9029785/>
- [33] Y. Ng, P. Van Goor, and R. Mahony, "Pose Observation for Second Order Pose Kinematics," *IFAC-PapersOnLine*, vol. 53, no. 2, pp. 2317–2323, 2020. <https://linkinghub.elsevier.com/retrieve/pii/S2405896320302640>



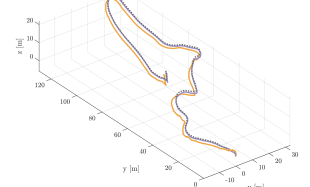
(a) Mars 01



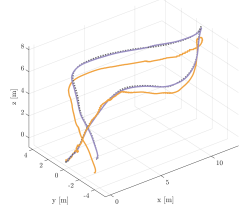
(b) Mars 02



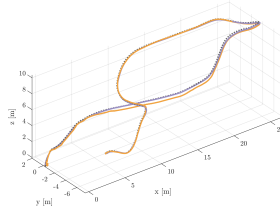
(c) Mars 03



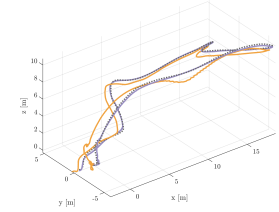
(d) Mars 04



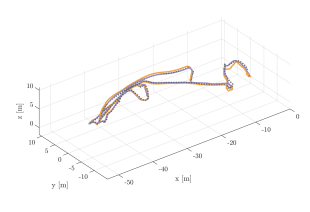
(e) Mars 05



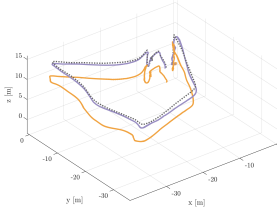
(f) Mars 06



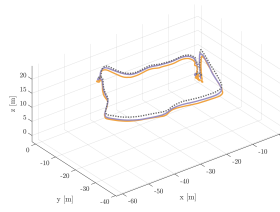
(g) Mars 07



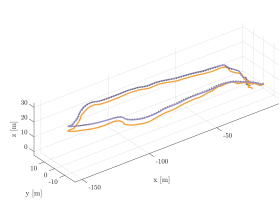
(h) Mars 08



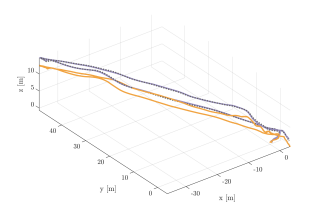
(i) Mars 09



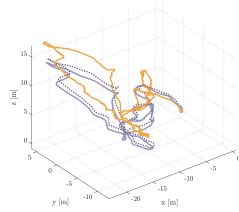
(j) Mars 10



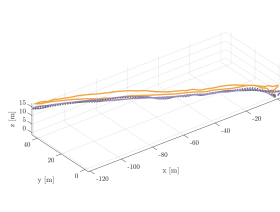
(k) Mars 11



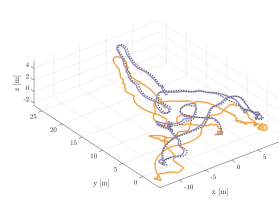
(l) Mars 12



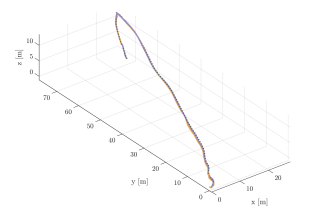
(m) Mars 13



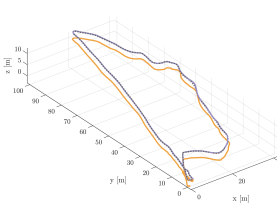
(n) Mars 14



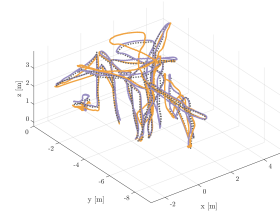
(o) Mars 15



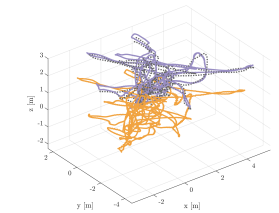
(p) Mars 16



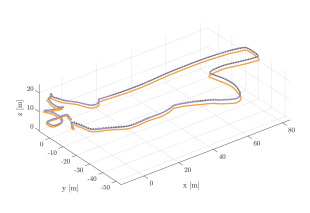
(q) Mars 17



(r) Mars 18



(s) Mars 19



(t) Outdoor 01

Fig. 5. Evaluation results of the **EqF** (purple) and a **MEKF** (yellow) framework on the *INSANE Dataset* [30]. As displayed in Table I the overall position error is relatively small given the trajectory lengths. Nonetheless, in most runs the EqF outperforms a MEKF implementation.